Ceramics International 48 (2022) 12048–12055

Contents lists available at ScienceDirect

Ceramics International

journal homepage: www.elsevier.com/locate/ceramint

Coexistence of antiferro- and ferrimagnetism in the spinel $ZnFe_2O_4$ with an inversion degree δ lower than 0.3

Miguel Ángel Cobos [a], Patricia de la Presa [a,b], Inés Puente-Orench [c,d], Irene Llorente [e], Irene Morales [a], Asunción García-Escorial [e], Antonio Hernando [a,b,f,g,h], José Antonio Jiménez [e,*]

[a] Instituto de Magnetismo aplicado (UCM-ADIF-CSIC), A6 22,500 Km, 28260, Las Rozas, Spain
[b] Dpto Física de Materiales, UCM, Ciudad Universitaria, 28040, Madrid, Spain
[c] Instituto de Nanociencia y Materiales de Aragón (INMA), CSIC-Universidad de Zaragoza, Zaragoza, 50009, Spain
[d] Institut Laue-Langevin, 71 Avenue des Martyrs, CS 20156, 38042, Grenoble CEDEX 9, France
[e] Centro Nacional de Investigaciones Metalúrgicas (CENIM-CSIC), Avda. Gregorio del Amo, 8, 28040, Madrid, Spain
[f] IMDEA Nanociencia, Madrid, 28049, Spain
[g] Donostia International Physics Center, Donostia, 20018, Gipuzkoa, Spain
[h] Universidad de Nebrija, Madrid, 28015, Spain

ARTICLE INFO

Keywords:
Spinel zinc ferrite
Inversion parameter
X-ray diffraction
Neutron powder diffraction
Rietveld refinement
Magnetic order

ABSTRACT

Samples with inversion parameter values (δ) ranging from 0.27 to 0.14 while maintaining the crystallite size value have been successfully fabricated from commercially available powders by mechanical grinding and thermal annealing treatments at temperatures ranging between 400 and 600 °C. Detailed characterization studies of these samples using X-ray, neutron diffraction and magnetic measurements have confirmed for the first time the simultaneous coexistence at 2 K of short range antiferromagnetic and ferrimagnetic ordering for a wide range of the inversion parameter. The magnetic phase diagram obtained is different from the one previously reported, which shows at 2 K the coexistence of long range antiferromagnetic order and short range order for values of inversion parameters less than 0.1 and the presence of a ferrimagnetic order only for values of $\delta > 0.2$. At room temperature, the Rietveld analysis of NPD patterns and the magnetization curves showed a paramagnetic behavior in the samples with $\delta \leq 0.1$. For the samples with higher cationic inversion, typical hysteresis curves of ferrimagnetic materials were observed and the saturation magnetization values obtained agree quite well with the net magnetic moment obtained from the Rietveld refinement of the neutron diffraction patterns.

1. Introduction

Oxide spinels comprise an important class of ternary compounds described by the chemical formula MM'_2O_4 [1], with a large variety of physical properties and applications in many areas of technology [2–7]. An ideal spinel structure is referred to the Fd-3m space group and it consists of a face centered cubic array of oxygen anions with one eighth of the tetrahedral (A) and one half of the octahedral interstices (B) occupied either with A^{2+} and B^{3+} cations. The cation distribution between A- and B-site leads to different long range ordering, which is characterized by the inversion degree δ defined as the fraction of trivalent cations at the A positions [8]. Depending on the cation arrangement, δ can vary from 0 to 1 in normal and inverse spinels respectively, assuming the value of 2/3 for a completely random arrangement.

Numerous investigations support that the equilibrium cation distribution of bulk zinc ferrites can be assumed to be completely normal ($\delta = 0$) [9]. This material is paramagnetic down to very low temperatures, with a transition temperature to antiferromagnetic (AFM) order of about 10 K [10]. However, depending on the sample preparation and thermal treatment, this phase can present a metastable cation distribution with some amount of Zn^{2+} residing at the octahedral site and the corresponding concentration of Fe^{3+} then occupying tetrahedral sites [11,12]. Associated with the partial exchange between cations, zinc ferrites can present super-paramagnetism or ferrimagnetism behaviour at room temperature [13,14]. The magnetic properties of the spinel ferrites are governed by the type of cations on the A and B sites and the magnetic interaction between them through the O^{2-} anions. It is elsewhere

* Corresponding author. Phone: +34 91 553 89 00; Fax: +34 91 534 74 25
E-mail address: jimenez@cenim.csic.es (J.A. Jiménez).

https://doi.org/10.1016/j.ceramint.2022.01.063
Received 14 May 2021; Received in revised form 26 November 2021; Accepted 6 January 2022
Available online 8 January 2022

reported that exist three possible kinds of super-exchange interactions, namely J_{AA}, J_{BB} and J_{AB} [15]. In general, the magnitude of the interaction energy depends on the distance of the cations to the oxygen ions and the angle formed by the bonds M-O-M' [16,17]. Considering the values of these two parameters, Néel stablished that in ferrites showing ferrimagnetism, the A-B interaction is predominant over A-A and B-B, and thus the net magnetic moment is the difference between the two average sublattice moments. The absence of paramagnetic cations at A sites in a zinc ferrite having the normal spinel structure would result in a weak AFM interaction within the Fe^{+3} cations at B sites below the Néel temperature.

The magnetic structure of equilibrium $ZnFe_2O_4$ is still not unequivocally determined despite almost 60 years of investigation. Köning et al. have reported the appearance of well resolved superlattice lines in neutron powder diffraction (NPD) patterns recorded at 4.2 K of well stoichiometric samples with small Fe^{2+} content [18]. Since these authors reported a Néel temperature of about 10 K, the additional lines would be associated with long range AFM ordering, which can be indexed on a tetragonal magnetic unit cell for which a is equal to the cubic unit cell and c is twice this value. However, several authors have found the absence of superlattice peaks associated with long range AFM order in many neutron studies performed with of $ZnFe_2O_4$ samples of varying quality below the Néel temperature [10,19]. Instead a well resolved and strong peak, they found broad diffuse peak located around the (1 0 1/2) reflection, thus indicating a short range order (SRO) [20]. As a B site is octahedrally coordinated with edge-shearing connectivity and the B-B distances are rather short, the supremacy of the nearest neighbor interaction will be much reduced, and the magnetic structure can adopt very complex orderings.

Both Hoffman et al. and Ehrhardt et al. have observed further features by neutron diffraction measurements between 2 and 535 K performed on coarse-grained $ZnFe_2O_4$ powders mechanically milled to obtain mean particle sizes ranging from 50 to 8 nm [21,22]. They reported that starting coarse grained samples present an antiferromagnetic long-range order (LRO) in the NPD patterns recorded at 2 K. When this sample was milled, they found a significant decrease in the AFM LRO reflection and the simultaneous appearance of a broad underlying hump in the same angle region, showing the coexistence of the antiferromagnetic LRO with a SRO. The intensity of this broad diffuse peak decreases with increasing the inversion parameter. After extensive grinding they observed that this peak disappears and intensity of the (111) reflection increases, which is indicative of the increase of a magnetic contribution at low temperature. These magnetic features are consistent with the AFM coupling of Fe^{3+} cations in tetrahedral and octahedral sites. These authors have included all these results in magnetic phase diagrams to explain evolution with the temperature of the magnetic behavior of the nanostructured $ZnFe_2O_4$ as functions of mean particle size or mean inversion parameter. These diagrams show several magnetic regions, but only one of them contains the coexistence of two simultaneous magnetic orders (antiferromagnetic LRO and SRO) for $\delta <$ 0.1 below 10 K. The rest of magnetic behavior regions in this diagram only include a magnetic order, which can be SRO, cluster glass or ferrimagnetic. In summary, the magnetic behavior at 2 K originates from the combination of AFM LRO and SRO at $\delta < 0.1$, which when increasing the inversion parameter gives way first to AFM SRO and for values higher than 0.2 to ferrimagnetism [21].

The objective of this work is to understand the relationship between the microstructural parameters determined by the Rietveld refinement and the magnetic behavior of the zinc spinel ferrite for values of the inversion parameter lower than 0.27 and from these results to evaluate the different magnetic orders present both at 2 K and at room temperature. For this goal, it is very important to compare very carefully the results obtained using XRD with those obtained from NPD to determine which microstructural parameter can be obtained with greater precision from each diffraction technique. Detailed characterization studies were performed on samples with inversion parameter values ranging from 0.27 to 0.14 while maintaining the crystallite size, using X-ray, neutron diffraction and magnetic measurements. Finally, it is expected to further clarify the effect of the cation distribution between A- and B-site on the saturation magnetization and its evolution with the temperature from the contribution of different superexchanges interactions.

2. Experimental procedure

Stoichiometric $ZnFe_2O_4$ particles with a low value of the inversion degree were obtained by the conventional ceramic synthesis (sample SC0) or annealing a commercial high purity zinc ferrite supplied by Alpha Aesar at 1100 °C for 2 h (sample COM 1100). For the conventional ceramic synthesis, a 1:1 M ratio mixture of ZnO and α-Fe_2O_3 (both 99% purity supplied by Alpha Aesar) was grounded to a very fine powder. The resulting powders were pressed into pellets with an uniaxial press and sintered at 1200 °C for 24 h. After this treatment, the samples were air cooled to room temperature. Finally, samples with different values of the inversion parameter were prepared from the commercial zinc ferrite by means of a mechanical milling process followed by an annealing treatment. For this goal, a certain amount of powder was introduced together with stainless steel balls of 10 mm into a stainless steel jar of 250 cm^3 in ball-to-powder weight ratio of 10:1 and then milled in a planetary ball mill Retsch PM4 at an average rotation speed of 275 rpm. The milling process was interrupted after 50 h since in a previous work it was confirmed that the inversion parameter was no further increased for higher times [12]. Then, milled powders were annealed for 1 h at 400, 500 and 600 °C (samples COM 50–400, COM 50–500 and COM 50–600, respectively).

The samples were initially characterized by powder XRD at Room Temperature (RT) using a Co radiation in a Bruker AXS D8 diffractometer equipped with a Goebel mirror and a LynxEye detector. XRD spectra were collected in Bragg-Brentano geometry using Co radiation (λ = 1.789 Å) over a range from 10 to 120° with a step width of 0.01° for avoiding Fe fluorescence. The nuclear and magnetic structure has been studied by means of NPD at 2 K and RT at Institut Laue Langevin, Grenoble (France) with the high flux D1B (λ = 2.52 Å) and the high resolution D2B (λ = 1.59 Å) diffractometers. D2B's detector has 128 cells spaced by 1.25° permitting to record the NPD pattern from $2\theta = 6°$ to 160° with an angular resolution of 0.05°. Powder samples were placed in vanadium cans of 5 mm in diameter and mounted onto a standard cryostat. Full diffraction patterns were obtained employing an acquisition time that was adjusted to obtain X-ray and neutron profiles of sufficient quality (optimal counting statistics). Thus, the average collecting time of high resolution NPD (D2B) was 3 h, while D1B data were collected in 30 min.

The obtained XRD and NPD patterns were analysed using the version 6.0 of the TOPAS (Bruker AXS). Because of the importance of using the precise wavelength value in these refinements, a separate measurement with the same instrument setup was performed with a standard of Si powders. The obtained diffraction pattern was fitted by fixing the lattice parameter of Si to 5.4308 Å and the incident neutron wavelength was refined. Background was built with a 12-term Chebychev polynomial. Then, Rietveld refinements were performed using as starting points the standardized structure for zinc ferrite taken from Pearson crystallographic database, where oxygen anions occupy 32e Wyckoff positions, whereas the Fe and Zn cations are located at 16c and 8b positions, respectively [23]. The refined parameters included only the lattice parameters (a), scale factors, the unique fractional coordinate of the oxygen atom ($u = x = y = z$), the degree of inversion δ (constraining the occupation of octahedral and tetrahedral sites to keep neutral the sample and to preserve the stoichiometric composition), background and two theta offset.

In spinels, the variation of the tetrahedral and octahedral bond distances associated with local inhomogeneity in the cation distribution can be similar to the dynamic displacements associated with thermal vibrations. Thus, the refined Debye-Waller factor (B) provides

information relating to the total magnitude of the local displacements, both static and dynamic components. Unfortunately, separating the thermal contribution to the atomic displacement parameter in a laboratory XRD measurement is far from trivial, as the analysis is entirely based on the angular decay of peak intensities. Thus, obtaining reliable data may not be possible since the accuracy of the refined B value is subject many factors like local variation of the inversion parameter, thermal diffusion scattering, dispersion, anomalous levels of incoherent scattering associated with fluorescence effects, dependence of the extinction factor on the mosaic crystal size … Some of these problems associated with laboratory XRD measurements can be overcome by using neutron radiation that offers the particular advantage that there is no angular dependence to the diffracted signal. The intensity of the NPD peaks within the same family should be the same after the correction of multiplicity, Lorentz and Debye-Waller factors when the system is paramagnetic and does not present a short-range order. However, a contribution from the magnetic structure at low 2 theta linked to the inversion parameter causes a high level of uncertainty in any evaluation of the local displacements within a sample from any observed decay of diffraction peak intensity. In other words: the correlation between the inversion parameter (occupancy) and Debye-Waller factor is too strong in our system to determine simultaneously both parameters from the Rietveld refinement. Therefore, the isotropic temperature factors (Biso) used in Rietveld refinements were fixed to the values reported by O'Neill to avoid unphysical values [9].

The determination of crystallite size and lattice strain simultaneously from line broadening of the XRD and NPD patterns has been carried out by the double Voigt approach [24]. For this analysis, the instrumental contribution to peak broadening was removed using the diffraction pattern of a corundum and $Na_2Ca_3Al_2F_{14}$ measured at room temperature by XRD and NPD, respectively. The errors quoted on these parameters are the estimated standard deviations produced by the Rietveld refinements. At this point, it should be noted that the results obtained for domain size and strain parameters present a limited reliability (ranging from 10 to 20%) associated with a large standard deviation.

In order to describe the intensity of the magnetic diffraction peaks in the case of the samples showing ferrimagnetic long range order at the diffraction temperature, an additional magnetic phase was included in the model used for the refinement of the NPD patterns by the Rietveld method. Thus, the nuclear contributions was calculated separately by using the spinel structure with the Fd-3m symmetry, together with a separate second phase that contains only the cations that contribute to the magnetic reflections. For this goal, it can be used a description of the magnetic structure in the spacer group P1 to refine all of the allowed magnetic modes. Since too many degrees of freedom have to be used in this approach to adjust the magnetic diffraction, and the zinc spinel ferrite only exhibits a limited number of magnetic reflections, the obtained magnetic moment can be quite inaccurate. Thus, it was selected and tested the Shubnikov BNS space-group R-3m' (166.101) for modelling the ferrimagnetic structure due to the analogy that exists between the structural properties of the zinc spinel with the Fe_3O_4, but considering the different arrangement of Fe cations in each case [25,26]. Besides, the lattice parameters of the magnetic phase were linked to the parent spinel and the scale factors were adjusted to take into account the difference in volume of both cells.

The quality and stability of the refinements were determined quantitatively by the Figures of Merits (FoM) or R-factors such as the statistically expected least-squares factor (Rexp), the weighted summation of residual of the least-squares fit (Rwp) and the goodness of fit (GoF or chi-square, whose limit tends to 1) [27].

Magnetic characterization as a function of applied field up to 5T has been performed using a standard superconducting quantum interference device (SQUID) MPMS (from Quantum Design) magnetometer. Hysteresis cycles have been measured at 5 and 300 K.

3. Results

3.1. Microstructural characterization

The reflection observed in the X-ray and D2B neutron diffraction patterns taken at RT in all samples studied match those of stoichiometric $ZnFe_2O_4$, as shown in Fig. 1 for the commercial high purity zinc ferrite annealed at 1100 °C. Only the sample prepared by the ceramic route showed some impurity peaks corresponding to ZnO, but in a mass fraction lower than 1%. It can be observed large differences in the relative intensities of the different peaks between XRD and ND patterns that are associated with differences between form factors and scattering lengths.

Although XRD and NPD can provide similar information, most of the structural results that have been published on spinel ferrites have been obtained using XRD, as NPD is a very expensive technique with limited access. Thus, it very important to evaluate and compare very carefully the results obtained by both techniques to determine if the results obtained by XRD are sufficient for the complete microstructural characterization of this material. On the other hand, it is very important to consider the trade-off between intensity and resolution when using a neutron source. The use of a high-resolution powder diffractometers such as the D2B is essential to refine a crystal structure, and for determining low differences in lattice parameters. In addition, it allows obtaining precise information on the microstructure of the sample from the analysis of peak shapes. However, the small number of these types of diffractometers available and the very slow data collection when using them, critically increase the pressure on instrument time and make the accessibility difficult. The choice of a general-purpose instrument such as the D1B can be an optimal solution, if the information obtained is

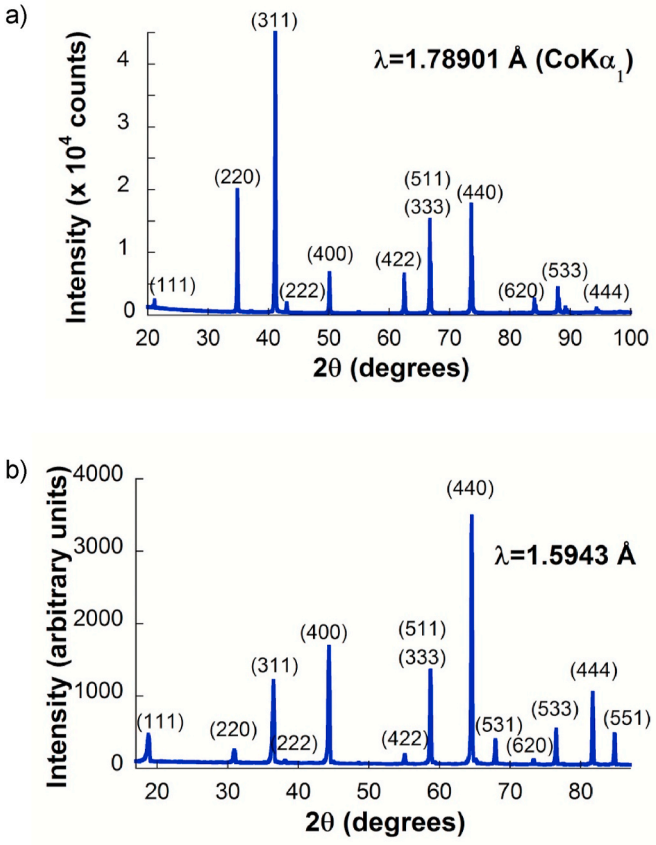

Fig. 1. Diffraction patterns recorded at room temperature of a commercial high purity sample annealed at 1100 °C (sample COM 1100) using a) laboratory x-ray and b) high resolution neutron sources.

complemented with that which can be obtained with greater precision in a conventional X-ray diffractometer. The values of the structural parameters and their standard deviations obtained from the Rietveld refinement of both XRD and NPD patterns are reported in Table 1. It is expected that neutron data will provide more reliable inversion parameters since between Zn and Fe there is a more noticeable difference between their neutron scattering lengths ($b_{Zn} = 5.68$ vs. $b_{Fe} = 9.45$ fm) than their X-ray scattering factors ($Z_{Zn} = 30$ vs. $Z_{Fe} = 26$) [28]. On the other hand, although the contribution to overall XRD scattering intensity by O is significant smaller in the presence of high Z elements like Fe and Zn, the neutron scattering length for this element is large ($b_O = 5.803$ fm). Thus, NPD is a better approach than XRD to determine the positions of oxygen atoms precisely. As shown in Table 1, the inversion parameter and the O-positions obtained from the NPD patterns recorded on both D1B and D2B diffractometers agree quite well. On the other hand, X-ray and D2B neutron data generally benefit from higher resolution, and therefore lattice parameters, crystallite size and lattice strain determined from their diffraction patterns coincide. It should be noted that as crystallite size and lattice strain are determined simultaneously from line broadening, it is expected a typical standard deviation for these parameters ranging from 10 to 20%. Although the reliability these parameter determined from the patterns recorded in the D1B diffractometer is sacrificed, it is a very valuable tool for studying the magnetic structure of this material since it allows obtaining high number of counts on a reasonable timescale.

The neutron diffraction data recorded in the D1B diffractometer at 2 K for all the samples investigated are represented in Fig. 2. In these figures, one can observe the presence of an additional highly asymmetric shaped broad and diffuse peak at 2θ between 10 and 20°. This feature

Table 1
Microstructural parameters obtained after Rietveld refinement of the diffraction patterns recorded using laboratory x-ray and neutron sources.

Sample	Lattice parameter (Å)	Inversion degree (δ)	O-Position (x = y = z)	Crystal. size (nm)	μ-deformation (ε)
COM 1100 XRD	8.4489 (5)	0.05 (1)	0.2416 (9)	>150	–
COM 1100 ND D2B	8.4498 (5)	0.05 (1)	0.2397 (3)	>150	–
SC0 XRD	8.4408 (5)	0.10 (1)	0.2398 (9)	>150	–
SC0 ND D1B	8.4436 (5)	0.09 (1)	0.2386 (3)	>150	–
SC0 ND D2B	8.4433 (5)	0.11 (1)	0.2398 (3)	>150	–
COM 50-600 XRD	8.4352 (5)	0.15 (1)	0.2411 (5)	18 (1)	0.0016 (2)
COM 50–600 ND D1B	8.4376 (5)	0.11 (1)	0.2406 (3)	19 (1)	0.0018 (2)
COM 50-500 XRD	8.4331 (5)	0.19 (1)	0.2415 (5)	16 (1)	0.0019 (3)
COM 50–500 ND D1B	8.4450 (5)	0.14 (1)	0.2413 (3)	21 (1)	0.0020 (2)
COM 50–500 ND D2B	8.4336 (5)	0.15 (1)	0.2411 (3)	15 (1)	0.0012 (4)
COM 50-400 XRD	8.4322 (5)	0.28 (2)	0.2424 (5)	15 (1)	0.0020 (2)
COM 50–400 ND D1B	8.4373 (5)	0.20 (2)	0.2414 (3)	14 (1)	0.0019 (2)
COM 50–400 ND D2B	8.4306 (5)	0.21 (1)	0.2414 (3)	15 (1)	0.0014 (4)

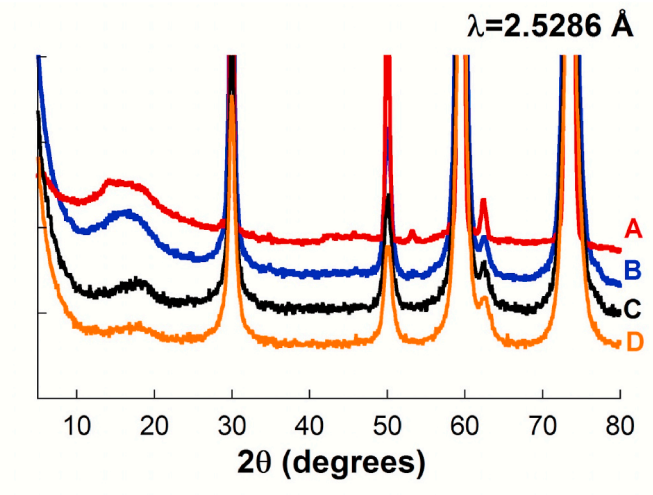

Fig. 2. Neutron diffraction patterns recorded at 2 K for the samples SC0 (A), COM 50–600 (B), COM 50–500 (C) and COM 50–400 (D).

vanished at temperatures above 10 K and it is absent in the measured recorded at RT. This may be the footprint of a short-range spin-spin AFM ordering. Then, it is obvious that the B-B super exchange interaction also comes into play for the magnetic properties below 10 K. It is worth to point out that the intensity of this broad peak decreased with the inversion degree of the spinel structure.

3.2. Bulk magnetization

The magnetic properties of the samples at 5 and 300 K were recorded up to maximum applied field of 50 KOe. As shown in Fig. 3 all magnetization curves are not saturated up to the maximum applied field. S-shaped hysteresis curves observed in this figure show the coexistence of two contributions: one characterized by a linear dependence of the magnetization due to the presence of a paramagnetic phase, and the other one with ferromagnetic-like behaviour, which was associated with a ferrimagnetic contribution that saturates at high fields. On the other hand, the samples COM 1100 and SC0 show only the paramagnetic component at 300 K.

In order to determine the saturation magnetization associated with the ferrimagnetic contribution, the paramagnetic one was subtracted considering that the magnetic susceptibility is the results of the sum of all magnetic contributions. Thus, it includes paramagnetic (PM), diamagnetic (DM), and ferrimagnetic components and at 5 K also an AFM one. As at high magnetic field (HF) the ferrimagnetic component is saturated, it can be discarded and only the paramagnetic, diamagnetic and AFM orderings vary with the applied field. In Table 2 is given the values for the saturation magnetization derived from the hysteresis curves. Comparing these results with the microstructural parameters of Table 1, it can be observed that the magnetization increases with increasing the inversion degree.

4. Discussion

In spinel structures, as both the crystallographic and magnetic unit cells are the same having identical symmetry relations, the nuclear and magnetic Bragg peaks occur at the same scattering angles. Therefore, the magnetic reflections superimposed the nuclear ones. From bulk measurements, we have concluded that our spinels can show a ferrimagnetic ordering. Due to strong form factor dependence with scattering angle, the magnetic contributions in the neutron diffraction pattern rapidly fall off for high reflection angles, and the additional contribution in the intensity occurs only at the lower 2 theta positions. Thus, discrepancies between the observed and calculated intensities in the (111), (220) and

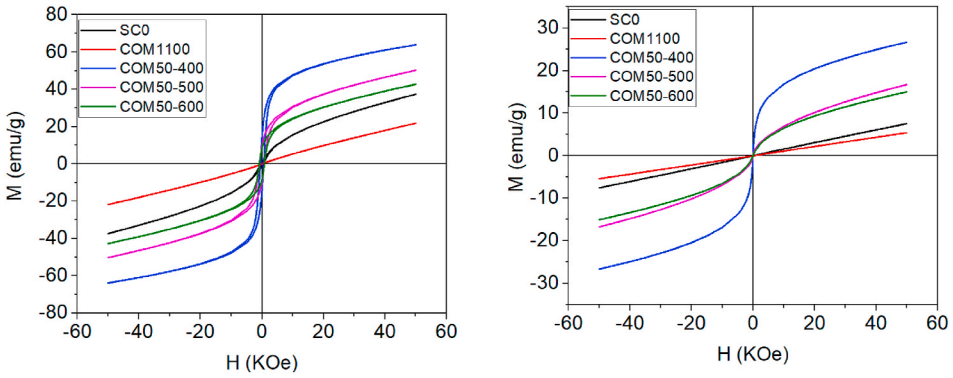

Fig. 3. M(H) curves recorded at 5 K (left panel) and 300 K (right panel) for the samples SC0, COM 1100 °C, COM 50–400, COM 50–500 and COM 50–600.

Table 2
Lattice parameters and magnetic moments at 300 and 2 K obtained by the combined analysis of the XRD and ND patterns recorded at 300 and 2 K and values of the saturation magnetization determined from the hysteresis curves.

Sample	Lattice Parameter (Å)	M_A (μ_B)	M_B (μ_B)	$M_S = \lvert M_B + M_A \rvert$	M_s (μ_B)
SC0 300 K	8.4410 (3)	–	–	–	0
SC0 2 K	8.4325 (3)	-1.17 (15)	1.9 (1)	0.7 (2)	0.65[a]
COM 50–600 300 K	8.4364 (5)	-1.4 (1)	1.6 (1)	0.2 (1)	0.27
COM 50–600 2 K	8.4279 (3)	-1.6 (2)	2.5 (1)	0.9 (2)	1.02[a]
COM 50–500 300 K	8.4376 (5)	-2.54 (15)	2.77 (8)	0.23 (17)	0.31
COM 50–500 2 K	8.4307 (3)	-2.78 (13)	4.00 (7)	1.22 (14)	1.36[a]
COM 50–400 300 K	8.4350 (5)	-2.57 (12)	3.22 (7)	0.65 (14)	0.77
COM 50–400 2 K	8.4311 (3)	-3.67 (7)	5.61 (3)	1.94 (8)	2.20[a]

[a] Measured at 5 K

(222) reflections may be found for the NPD when this order is present, as observed in Fig. 4 for the refinement of ND pattern recorded at 2 K on the D1B diffractometer with the 50-COM 400 sample.

When both magnetic and nuclear Bragg reflections coincide, it is not so obvious to separate both contributions. The high correlation between the contribution associated with cation occupancies and magnetic moments may lead to unsatisfactory fits, and to differences between the inversion parameter determined by the Rietveld refinement of the XRD and NPD patterns. Comparing the results shown in Tables 1 and 2, it is observed an increase with δ of both, the difference between the value of the inversion degree determined from the refinement of the XRD and NPD patterns and the saturation magnetization associated with the ferrimagnetic contribution. Thus, it was concluded that discrepancies among some microstructural parameters obtained by the Rietveld refinement of both types of diffraction data may arise from an increase on the magnetic scattering contribution with δ associated with the strong magnetic interaction between Fe^{3+} cations on A and B sites antiferromagnetically coupled.

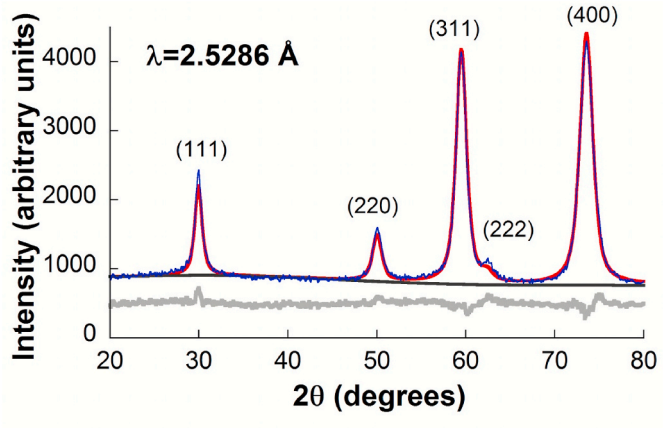

Fig. 4. Comparison of the observed (blue solid line) and calculated (red line) ND pattern obtained after Rietveld refinement of the ND pattern obtained at 2 K on the D1B diffractometer for the COM 50–400 sample. The differences between experimental data and the fitted simulated pattern are plotted as a continuous grey line at the bottom. (For interpretation of the references to colour in this figure legend, the reader is referred to the Web version of this article.)

The refinement of the NPD and XRD data alone have provide different values for some microstructural parameters because the different interaction mechanisms of the neutron and the X-ray with the sample makes the uniqueness of a result obtained sometimes questionable. This problem can be eliminated by the simultaneous Rietveld refinement of both diffraction patterns, including a magnetic phase in the refinement of the neutron data to account for the magnetic contribution that may appears when some Fe^{3+} magnetic ions are occupying also A sites. Although annealing at high temperature may lead to cations reordering and changes on the crystallite size and microstrain, Hoffman et al. have reported that in nanostructured $ZnFe_2O_4$ samples microstructural parameters like inversion degree, fractional coordinate of the oxygen atom and particle size remain unchanged up to ~525 K compared with the value at room temperature [21]. Thus, these parameters were simultaneous refined and constrained to the same value for the patterns recorded at both 300 and 2 K using laboratory x-ray and neutron sources. The value of the lattice parameters at room temperature was also constrained to be the same both for XRD and NPD profiles, but it was set as a variable both, the sample displacement correction in the XRD pattern and zero shift error in the NPD pattern, to include an extra degree of freedom to the peak positions. Besides, independent magnetic moments were included in the refinement for the NPD data recorded at 300 and 2 K under the assumption that the cation distribution in the magnetic structure at both temperatures is the same. As the Shubnikov BNS space-group R-3m′ was used for the refinement of the magnetic structure, two values for the magnetics moments were obtained: M_A for the cations at the tetrahedral positions and M_B for the octahedral Fe(2a) and Fe(2b) cations in Wyckoff positions 3b and 9e. The best-fitted microstructural parameters obtained by the combined analysis after Rietveld refinement of the XRD and NPD patterns recorded at 300 and 2 K are given in Tables 2 and 3. As shown in Table 3, the good quality of these fits is accompanied by low values of the R-factors and GoF.

The refinement NPD data showed that the spins at A and B sites are aligned anti-parallel, suggesting that the magnetic structure is

Table 3
Values obtained for the microstructural parameters constrained to the same value in the combined analysis of the patterns recorded at both 300 and 2 K using laboratory x-ray and neutron sources.

Sample	Inversion degree (δ)	O-Position (x = y = z)	Crystal. size (nm)	μ-defor-mation (ε)	R_{WP}	R_{exp}	GoF
SC0	0.10 (1)	0.2398 (1)	>150	–	2.79	8.27	2.96
COM 50-600	0.14 (1)	0.2408 (1)	17.4 (5)	0.0016 (1)	3.12	2.47	1.26
COM 50-500	0.18 (1)	0.2414 (1)	16.5 (5)	0.0019 (1)	3.51	2.70	1.30
COM 50-400	0.27 (1)	0.2419 (1)	14.1 (5)	0.0019 (1)	3.27	2.65	1.26

ferrimagnetic. It can be observed in Table 2 that all samples present a net magnetic moment at 2 K, but at room temperature only the COM 50–400, COM 50–500 and COM 50–600 samples present a net magnetic moment. Although the magnetic moments of the SC0 sample were included as parameters to be refined in the Rietveld analysis of its NPD pattern measured at 300 K, a value of ≈0 was obtained for both, M_A and M_B, in agreement with the paramagnetic behaviour observed at 300 K in Fig. 3 for this sample.

Fig. 3 also shows that COM 50–400, COM 50–500 and COM 50–600 samples present at 300 K S-shaped hysteresis curve typical of a ferrimagnetic response characterized by the absence of coercivity and remanent magnetization. Cobos et al. using the ZFC–FC procedure have reported a blocking temperature (TB) below room temperature for zinc ferrite samples characterized by crystallite size and inversion degree similar to those reported in Table 2 for these three samples [14]. The thermal energy will be sufficient to suppress ferromagnetic (FM) behaviour of the particles of these three samples at room temperature. Thus, they become superparamagnetic, which means that although their magnetization curves do not show hysteresis, they magnetization values (Ms, M_A and M_B) are typical of ferromagnetic substances.

The distances between the magnetic ions along with the M-O-M' angles play a crucial role in determining the magnetic exchange interactions, and therefore greatly affect the magnetic characteristics. As the inversion parameters increases, it can be observed in Tables 1 and 3 that the fractional coordinate of the oxygen atom also increases due to the adjustment of the structure to accommodate differences in the effective radii of the cations in the tetrahedral and octahedral sites. Thus, the Fe^{3+}-O-Fe^{3+} angles associated with the A-B and B-B interactions that are determined from the refined structural model varies, respectivley, from 121.8 and 94.8° in the sample with δ = 0.05 to 122.5 and 93.8° in the sample with δ = 0.27. According to the semiempirical rules reported by Goodenough and Kanamori [29,30], a bond angle above 120° results in an strong AFM coupling between the Fe^{3+} cations on octahedral and tetrahedral lattice sites. These rules also predict a weak FM superexchange interaction between Fe^{+3} cations on the octahedral B-sites under angle of ~ 90°. However, the increase of this angle to values higher than ~ 94° for δ ≤ 0.27 determines that coupling between Fe^{3+} cations on B sites can varies from FM to AFM, making it possible to observe macroscopically the existence of an AFM order in both, the NPD patterns and the magnetic measurements recorded at 2 and 5 K, respectively.

It is obvious that the degree of inversion plays an important role for the magnetic properties. In the absence of inversion, it is present only the AFM superexchange B-B interaction, i.e. the AFM coupling between the Fe cation which occupies only octahedral positions. When some Zn cations from tetrahedral sites are exchanged with Fe, this cationic inversion results in the formation of a local AFM coupling between Fe ions at tetrahedral sites with their closest neighbors Fe at octahedral positions. It is elsewhere reported that the A-B interaction is the strongest nearest-neighbor magnetic coupling in spinel ferrites. Uhl et al. have calculated theoretically that in magnetite the second strongest superexchange coupling occurs ferromagnetically between two nearest-neighbors Fe cations, both at the octahedral site [31]. Thus, the AFM interaction between Fe cations located on octahedral and tetrahedral sites can locally induce the formation of FM coupling between the neighboring Fe cations on octahedral sites. The formation of local FM coupling between Fe ions at octahedral sites in a nominally antiferromagnetic zinc ferrite has been confirmed by Rodríguez Torres et al. [32]. This would cause an extended superexchange interaction B-O-A-O-B that gives rise to a ferrimagnetic ordering. The existence of third-neighbor Fe^{3+} spins coupled antiferromagnetically has been also pointed out by Kamazawa et al. from their measurements on a single crystal of $ZnFe_2O_4$ [33].

It has been reported in previous works that spinel zinc ferrite can present AFM or ferrimagnetic order depending on the inversion parameter [12–14]. NPD data confirm that both, short range (SRO) and long range (LRO) antiferromagnetic order can coexists at 2 K for values of the inversion parameter lower than 0.1 [21,22]. These studies have also shown that at this temperature an increase in inversion led first to AFM SRO and to a ferrimagnetic state for values greater than 0.2. However, we have confirmed for first time that both short range antiferromagnetic and ferrimagnetic ordering can coexist simultaneously at 2 K for values of the inversion parameter ranging from 0.05 to about 0.3. As the inversion parameter is increased, it can be observed in the NPD of Fig. 5 that the intensity of the FM like contribution increases and therefore the magnetization obtained by both, the M − H curve and Rietveld refinement, shown in Table 2. On the other hand, Fig. 2 shows that this increases in the FM like ordering is accompanied by a decrease in the intensity of the broad peak associated with the AFM ordering. It can be concluded that there is a local competition in the structure between the AFM and FM coupling of Fe cations at the octahedral sites induced by the AFM superexchange A-B interaction.

As the A–B superexchange interaction is significantly stronger than the B-B, higher thermal energy is required to overcome it and disorient the magnetic moments. We consider that the FM component dominates at high temperature, but the AFM B-B component gradually will be strengthened at low temperature, giving rise to a competition with the third-neighbor AFM interactions B-A-B. As a result, the magnetic structure may become magnetically frustrated and the system magnetically inhomogeneous, causing that the AFM long range order (LRO) would be suppressed [34]. Thus, below the Néel temperature small antiferromagnetic domains and disordered domain walls could form.

5. Conclusions

The main result of the structural and magnetic characterization performed in the spinel $ZnFe_2O_4$ can be summarized as follows:

(1) XRD and NPD data alone have been used to characterize the microstructure present in this material, but different values for some microstructural parameters can be obtained due to the different interaction mechanisms of the neutron and the X-ray with the sample. This problem has been be eliminated by the simultaneous Rietveld refinement of both diffraction patterns, including a magnetic phase in the refinement of the neutron data to account for the magnetic contribution that may appears when some Fe^{3+} magnetic ions are occupying also A sites.
(2) Unlike previous studies, we have confirmed for the first time the simultaneous coexistence at 2 K of short range antiferromagnetic and ferrimagnetic ordering when the inversion degree δ is lower than ~0.3. The neutron diffraction patterns recorded at this temperature showed a diffuse peak at low angles associated with

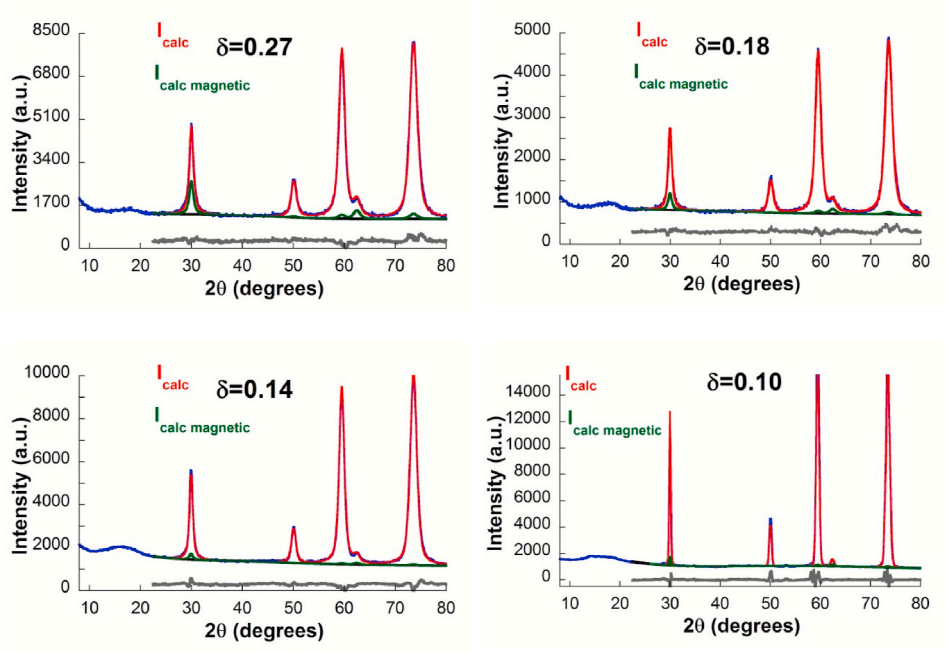

Fig. 5. Comparison of the observed (blue solid line) and calculated (red line) ND pattern obtained after Rietveld refinement of the ND patterns recorded at 2 K for different samples sample with the green line indicating the magnetic contribution to the fitted model. The differences between experimental data and the fitted simulated pattern are plotted as a continuous grey line at the bottom. (For interpretation of the references to colour in this figure legend, the reader is referred to the Web version of this article.)

short range antiferromagnetic B-B interaction and the Rietveld refinement of these patterns confirmed the presence of a ferromagnetic like order that was associated with an extended superexchange antiferromagnetic B-A-B interaction.

(3) Although both ordering are present at 2 K, the antiferromagnetic contribution decreases and the ferrimagnetic contribution increases as the inversion degree increases. As a result of the competition between these two interactions, it may be originated frustration in the magnetic structure that causes the suppression of the antiferromagnetic long range order (LRO).

(4) At room temperature, the samples with $\delta \leq 0.1$ behave paramagnetic, while for the samples with higher cationic inversion, typical hysteresis curves of ferrimagnetic materials were recorded, characterized by the absence of coercivity and remanent magnetization. Due to a crystallite size lower than 20 nm, ferrimagnetic zinc ferrite particles can behave superparamagnetically at RT.

Declaration of competing interest

The authors declare that they have no known competing financial interests or personal relationships that could have appeared to influence the work reported in this paper.

Acknowledgements

The authors acknowledge ILL and the D1B-CRG (Ministerio de Ciencia, e Innovación, Spain) for the beam time allocated at both the D1B and D2B instruments (Jose A. Jimenez; M.A.COBOS; LLORENTE CARRASCO Irene and PUENTE ORENCH Ines. (2020). Effect of inversion degree on the magnetic properties of spinel zinc ferrite. Institut Laue-Langevin (ILL) doi:10.5291/ILL-DATA.CRG-2710; Jose A. Jimenez; M.A.COBOS; LLORENTE CARRASCO Irene; NASSIF Vivian and PUENTE ORENCH Ines. (2021). Evolution of the magnetic properties with annealing temperature of spinel zinc ferrite disordered by ball milling. Institut Laue-Langevin (ILL) doi:10.5291/ILL-DATA.CRG-2797, Jose A. Jimenez; M.A.COBOS; LLORENTE CARRASCO Irene and PUENTE ORENCH Ines. (2020). Effect of microstructural features and defects introduced by mechanical milling and thermal treatments on the magnetic order of spinel zinc. Institut Laue-Langevin (ILL) doi:10.5291/ILL-DATA.5-31-2742). This research has been funded by Spanish Ministries of Science and Innovation (MICINN) and of Economy and Competitiveness (MINECO) by means of the AFORMAR (PID2019-109334RB) and RTI2018-095856-B-C21 projects, respectively. The support of the grants from the Community of Madrid number S2018/NMT-4381-MAT4.0-CM and P2018/NMT-4321 is also recognized.

References

[1] R.J. Hill, J.R. Craig, G.V. Gibbs, Systematics of the spinel structure type, Phys. Chem. Miner. 4 (1979) 317–339, https://doi.org/10.1007/BF00307535.

[2] A. Bhaskar, S.R. Murthy, Effect of sintering temperatures on the elastic properties of Mn (1%) added MgCuZn ferrites, J. Magn. Magn Mater. 355 (2014) 100–103, https://doi.org/10.1016/j.jmmm.2013.11.053.

[3] H. Bahiraei, M.Z. Shoushtari, K. Gheisari, C.K. Ong, The effect of sintering temperature on the electromagnetic properties of nanocrystalline MgCuZn ferrite prepared by sol–gel auto combustion method, Mater. Lett. 122 (2014) 129–132, https://doi.org/10.1016/j.matlet.2014.02.027.

[4] M.B. Mohamed, A.M. Wahba, Structural, magnetic, and elastic properties of nanocrystalline Al-substituted Mn0.5Zn0.5Fe2O4 ferrite, Ceram. Int. 40 (2014) 11773–11780, https://doi.org/10.1016/j.ceramint.2014.04.006.

[5] S. Güner, S. Esir, A. Baykal, A. Demir, Y. Bakis, Magneto-optical properties of Cu1−xZnxFe2O4 nanoparticles, Superlattice. Microst. 74 (2014) 184–197, https://doi.org/10.1016/j.spmi.2014.06.021.

[6] S. Chakrabarty, M. Pal, A. Dutta, Structural, optical and electrical properties of chemically derived nickel substituted zinc ferrite nanocrystals, Mater. Chem. Phys. 153 (2015) 221–228, https://doi.org/10.1016/j.matchemphys.2015.01.006.

[7] P. Chavan, L.R. Naik, X-ray diffraction studies and dielectric properties of Ni doped Mg ferrites, Vacuum 152 (2018) 47–49, https://doi.org/10.1016/j.vacuum.2018.03.007.

[8] H.S.C. Oneill, A. Navrotsky, Simple spinels: crystallographic parameters, cation radii, lattice energies, and cation distribution, Am. Mineral. 68 (1983) 181–194. https://pubs.geoscienceworld.org/msa/ammin/article-abstract/68/1-2/181/41446/Simple-spinels-crystallographic-parameters-cation.

[9] H.S.C. Oneill, Temperature dependence of the cation distribution in zinc ferrite (ZnFe2O4) from powder Xrd structural refinements, Eur. J. Mineral 4 (1992) 571–580, https://doi.org/10.1127/ejm/4/3/0571.

[10] J.M. Hastings, L.M. Corliss, An antiferromagnetic transition in zinc ferrite, Phys. Rev. 102 (1956) 1460–1463, https://doi.org/10.1103/physrev.102.1460.

[11] C. Yao, Q. Zeng, G.F. Goya, T. Torres, J. Liu, H. Wu, M. Ge, Y. Zeng, Y. Wang, J. Z. Jiang, ZnFe2O4 nanocrystals: synthesis and magnetic properties, J. Phys. Chem. C 111 (2007) 12274–12278, https://doi.org/10.1021/jp0732763.

[12] M.A. Cobos, P. de la Presa, I. Llorente, A. García-Escorial, A. Hernando, J. A. Jiménez, Effect of preparation methods on magnetic properties of stoichiometric zinc ferrite, J. Alloys Compd. 849 (2020), 156353, https://doi.org/10.1016/j.jallcom.2020.156353.

[13] S.J. Stewart, I.A. Al-Omari, F.R. Sives, H.M. Widatallah, Non-equilibrium cation influence on the Neel temperature in ZnFe2O4, J. Alloys Compd. 495 (2010) 506–508, https://doi.org/10.1016/j.jallcom.2009.10.258.

[14] M.A. Cobos, P. de la Presa, I. Llorente, J.M. Alonso, A. García-Escorial, P. Marín, A. Hernando, J.A. Jiménez, Magnetic phase diagram of nanostructured zinc ferrite as a function of inversion degree δ, J. Phys. Chem. C 123 (2019) 17472–17482, https://doi.org/10.1021/acs.jpcc.9b02180.
[15] L. Néel, Propriétés magnétiques des ferrites: ferrimagnétisme et antiferromagnétism, Ann. Phys. Paris 3 (1948) 137–198, https://doi.org/10.1051/anphys/194812030137.
[16] E.W. Gorter, Saturation magnetization and crystal chemistry of ferramagnetic oxides, Philips Res. Rep. 9 (1954) 295–320. https://www.pearl-hifi.com/06_Lit_Archive/02_PEARL_Arch/Vol_16/Sec_53/Philips_Rsrch_Reports_1946_thru_1977/Philips%20Research%20Reports-09-1954.pdf.
[17] E.W. Gorter, Saturation magnetization and crystal chemistry of ferramagnetic oxides, 2. Theory of ferrimsgnetism, Philips Res. Rep. 9 (1954) 321–365. https://www.pearl-hifi.com/06_Lit_Archive/02_PEARL_Arch/Vol_16/Sec_53/Philips_Rsrch_Reports_1946_thru_1977/Philips%20Research%20Reports-09-1954.pdf.
[18] U. König, E.F. Bertaut, Y. Gros, M. Mitrikov, G. Chol, Models of the magnetic structure of zinc ferrite, Solid State Commun. 8 (1970) 759–764, https://doi.org/10.1016/0038-1098(70)90425-4.
[19] P.W. Anderson, Ordering and antiferromagnetism in ferrites, Phys. Rev. 102 (1956) 1008–1013, https://doi.org/10.1103/physrev.102.1008.
[20] M.K. Fayek, J. Leciejewicz, A. Murasik, I.I. Yamzin, Antiferromagnetism of Zn0.87Mn0.13Fe2O4, Phys. Status Solidi B 37 (1970) 843–850, https://doi.org/10.1002/pssb.19700370235.
[21] M. Hofmann, S.J. Campbell, H. Ehrhardt, R. Feyerherm, The magnetic behaviour of nanostructured zinc ferrite, J. Mater. Sci. 39 (2004) 5057–5065, https://doi.org/10.1023/b:jmsc.0000039185.80910.59.
[22] H. Ehrhardt, S.J. Campbell, M. Hofmann, Magnetism of the nanostructured spinel zinc ferrite, Scripta Mater. 48 (2003) 1141–1146, https://doi.org/10.1016/s1359-6462(02)00598-5.
[23] P. Villars, K. Cenzual, Pearson's Crystal Data: Crystal Structure Database for Inorganic Compounds, ASM International, Materials Park, Ohio, 2020/2021. https://www.asminternational.org/materials-resources/online-databases/pearson/-/journal_content/56/10192/6382084/DATABASE.
[24] D. Balzar, H. Ledbetter, Voigt-function modeling in Fourier analysis of size- and strain-broadened X-ray diffraction peaks, J. Appl. Crystallogr. 26 (1993) 97–103, https://doi.org/10.1107/s0021889892008987.
[25] P.S. Whitfield, Quantitative phase analysis of challenging samples using neutron powder diffraction. Sample #4 from the CPD QPA round robin revisited, Powder Diffr. 31 (2016) 192–197, https://doi.org/10.1017/s088571561600021x.
[26] P. Wright, A.M. Bell, J.P. Attfield, Variable temperature powder neutron diffraction study of the Verwey transition in magnetite Fe_3O_4, Solid State Sci. 2 (2000) 747–753, https://doi.org/10.1016/s1293-2558(00)01107-9.
[27] V.K. Pecharsky, P.Y. Zavalij, Fundamentals of Powder Diffraction and Structural Characterization of Materials, Springer, New York, 2005, https://doi.org/10.1007/b106242.
[28] S.W. Lovesey, Theory of Neutron Scattering from Condensed Matter, vol. 1, Clarendon Press, Oxford, 1984. Nuclear scattering, https://global.oup.com/academic/product/theory-of-neutron-scattering-from-condensed-matter-9780198520283?lang=en&cc=in.
[29] J.B. Goodenough, Magnetism and the Chemical Bond, Interscience Publishers, New York, 1963, https://doi.org/10.1002/bbpc.19640681015.
[30] J. Kanamori, Superexchange interaction and symmetry properties of electron orbitals, J. Phys. Chem. Solid. 10 (1959) 87–98, https://doi.org/10.1016/0022-3697(59)90061-7.
[31] M. Uhl, B. Siberchicot, A first-principles study of exchange integrals in magnetite, J. Phys. Condens. Matter 7 (1995) 4227–4238, https://doi.org/10.1088/0953-8984/7/22/006.
[32] C.E. Rodríguez Torres, G.A. Pasquevich, P. Mendoza Zélis, F. Golmar, S.P. Heluani, Sanjeev K. Nayak, Waheed A. Adeagbo, Wolfram Hergert, Martin Hoffmann, Arthur Ernst, P. Esquinazi, S.J. Stewart, Oxygen-vacancy-induced local ferromagnetism as a driving mechanism in enhancing the magnetic response of ferrites, Phys. Rev. B 89 (2010), 104411, https://doi.org/10.1103/physrevb.89.104411.
[33] K. Kamazawa, Y. Tsunoda, H. Kadowaki, K. Kohn, Magnetic neutron scattering measurements on a single crystal of frustrated ZnFe2O4, Phys. Rev. B 68 (2003), 024412, https://doi.org/10.1103/physrevb.68.024412.
[34] J.A. Mydosh, Spin glasses: redux: an updated experimental/materials survey, Rep, Prog. Phys. 78 (2015), 052501, https://doi.org/10.1088/0034-4885/78/5/052501.